Mechanical properties of connected carbon nanorings via molecular dynamics simulation

Nan Chen and Mark T. Lusk*
Colorado School of Mines

Adri C. T. van Duin and William A. Goddard III
California Institute of Technology
(Received 1 March 2005; published 4 August 2005)

Stable, carbon nanotori can be constructed from nanotubes. In theory, such rings could be used to fabricate networks that are extremely flexible and offer a high strength-to-density ratio. As a first step towards realizing such *nanochains* and *nanomaile*, the mechanical properties of connected carbon nanorings were investigated via molecular dynamics simulation. The Young's modulus, extensibility and tensile stength of nanorings were estimated under conditions that idealize the constraints of nanochains and nanomaile. The results indicate nanorings are stable under large tensile deformation. The calculated Young's modulus of nanorings was found increase with deformation from 19.43 GPa to 121.94 GPa (without any side constraints) and from 124.98 GPa to 1.56 TPa (with side constraints). The tensile strength of unconstrained and constrained nanorings is estimated to be 5.72 and 8.522 GPa, respectively. The maximum strain is approximately 39% (nanochains) and 25.2% (nanomaile), and these deformations are completely reversible.

DOI: 10.1103/PhysRevB.72.085416 PACS number(s): 81.07.−b, 81.07.De, 61.46.+w

I. INTRODUCTION

A topic of current interest is how elementary carbon nanostructures might best be used in the design of macroscopic material structures with optimized mechanical performance.[1] For instance, carbon nanotubes (CNT's) synthesized by a variety of methods in both single-wall (SWNT) and multiwall (MWNT) structures[2,3], are being considered as reinforcement fibers in epoxy resins. This is attractive since CNT's have a Young's modulus on the order of 1 TPa (Ref. 4) and can sustain high interfacial shearing stresses.[5] Such composites may some day offer significant advantages over carbon reinforced resins currently used in industry.[5–7] Other approaches for mechanical design using CNT's include relatively thick matts of SWNT's called *Bucky paper*[8] and composite CNT-polymer nanofibers. Nanofibers and ribbons have been fabricated from SWNT's[1,9], which have been subsequently embedded in polymer sheets[10] and textiles.[11]

CNT's have certainly received the bulk of attention thus far as elementary construction components, but other carbon nanostructures may offer additional choices in designing materials with optimized mechanical performance. *Bucky balls*,[12] for instance, are being investigated as possible lubricants,[13] and carbon *nanohooks* can be used to make nanovelcro.[14] Unique mechanical properties associated with *nanohorns*[15] and *nanojunctions*[16] may also lead to materials synthesized with specialized mechanical properties. Of particular interest in the current investigation, though, are the mechanical properties of nanotori. Also known as *nanorings,* these closed structures have been considered theoretically for some time where the focus has been on the stability of individual rings. Earlier investigations focused on tori fabricated with a series of heptagon-pentagon defects;[17–19] more recently, perfect toroidal polyhexes[20] have been modeled wherein the ends of a SWNT are brought together to form a toroid free of any defects.[21–23]

In parallel with these computational studies of stability, nanorings have been experimentally fabricated by a number of researchers.[25–29] As shown in Fig. 1, such *nanorings* have also been observed to form in linked arrangements.[28] Based on their size, most of the nanorings observed must be composed of multiwall nanofibers, but there is some indication that perfect nanotori are formed as well.

To the best of our knowledge, the response of nanorings to an applied load has not yet been studied. This information is a necessary first step in determining how these tori may best be used to construct materials with optimized mechanical properties. For instance, nanorings might be embedded in resin sheets or fibers. Even more exotic, though, would be the construction of *nanochains* and two-dimensional structures, *nanomaile*, as illustrated in Figs. 2 and 3, which are constructed by linking such rings together. The fabrication of such structures, while daunting, would obviate the need to use resins; the reduced mass and mechanical response are strong motivators for at least considering the possibility of creating these ring networks.

Molecular dynamics investigations figure prominently in quantifying the mechanical response of nanostructures. In

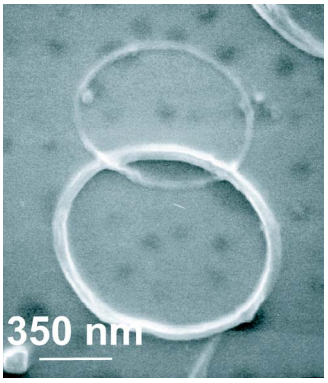

FIG. 1. (Color online) Experimentally created nanorings. (Reprinted from Ref. 28 with permission from Elsevier.)

 ©2005 The American Physical Society

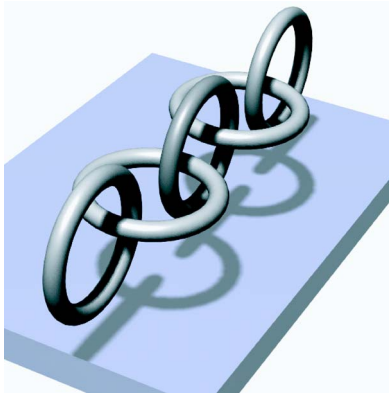

FIG. 2. (Color online) Illustration of a nanochain constructed of CNT's.

addition to the studies already noted, MD analyses have been employed to estimate the Young's modulus of SWNT's,[30] to elucidate the roles of methane and neon on the mechanical properties of nanotubes,[31] to quantify the elastic and plastic properties of MWNT's,[32,33] and to study CNT compression.[34,35] The force fields employed in these investigations are based on the Brenner empirical bond order potential.[34,36–41] However, the Brenner potential does not include long range interaction such as van der Waals and Coulomb interactions, and a Lennard-Jones term was typically introduced to account for these effects.

Accurate geometry of ground state hydrocarbons can be predicted with Brenner or modified Brenner potentials. However, the shape of the potential curve (energy versus atomic distance) for bond breaking and reaction is not captured accurately.[42] Recently, though, a general bond-order-dependent reactive force field (ReaxFF) (Ref. 43) was developed by van Duin *et al.* which includes long range interactions and bond dissociation. Reaction parameters are obtained by fitting potential curves to quantum chemistry (QC) calculations.[42] ReaxFF provides an accurate description of hydrocarbon bond dissociation and reaction, geometry, and heats of formation. In addition, it accurately captures quantum mechanical transition state energies—crucial for describing the formation and the failure of nanostructures.[44]

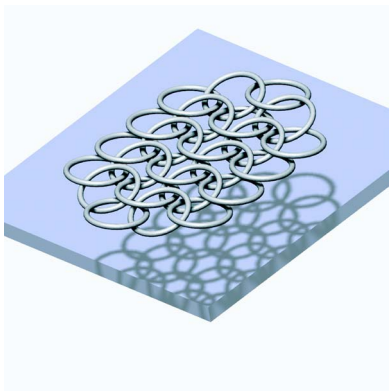

FIG. 3. (Color online) A two-dimensional ring structure in a 4-in-1 weave of nanomaile.

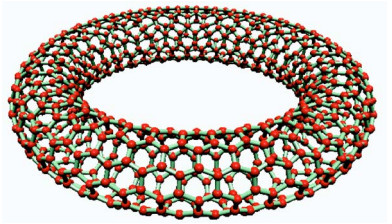

FIG. 4. (Color online) Isometric view of the initial structure of a CNT nanoring. The nanoring was constructed from a perfect (5,5) nanotube.

In the current work, the ReaxFF method was used to quantify the mechanical properties of simple nanoring and nanomaile structures. In order to ensure the accuracy of the tool for carbon nanostructures, the Young's modulus of a SWNT was first calculated, and a nanoring structure was equilibrated to verify its stability. The simulator was then used to calculate the Young's modulus, tensile strength and maximum strain of nanorings under two types of loading.

II. APPROACH

ReaxFF provides a good description for the physical and chemical properties of carbon hydrides, and the molecular dynamics calculations presented in this paper utilize this force field methodology to study nanotori. Details of the force field method and model parameters associated with carbon-carbon bonds can be found elsewhere.[42]

A. Validation of the force field model

The Young's modulus of SWNT's is well known both through experiments and theoretical calculations, and ReaxFF was applied to this geometry in order to generate an elastic constant for comparison. A (10, 10) nanotube with a length of 35.9 Å was equilibrated at 30 K for 5 ps and was then put under tension at a constant loading rate (4.45×10^{10} s). The simulation was carried out in 0.25 fs steps at 30 K in order to ensure that the carbon atoms had sufficient kinetic energy to reach equilibrium position.

B. Geometry of an equilibrated nanoring

The initial structure for all calculations was taken to be a perfect toroid created by closing a (5, 5) CNT of armchair chirality with 50 unit cells (1000 carbon atoms). This ring, shown in Fig. 4, is not in equilibrium since bonds on the outer surface are stretched relative to those closer to the center, and its evolution has been investigated previously using a Brenner-Tersoff potential.[23] It was reported that a kinked structure developed, and so it was particularly important to determine whether this kinking is also observed within the ReaxFF paradigm. The nanoring was therefore annealed for 25 ps at 500 K in order to judge its stability. This process was repeated for ring structures with 30, 40, 65, 85, and 100 units cells in order to quantify the change in structural stability with CNT length.

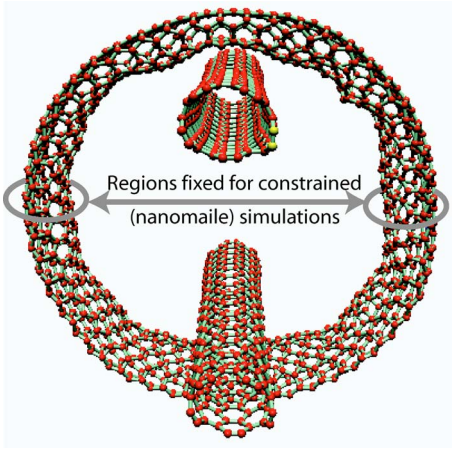

FIG. 5. (Color online) Structure used for tensile testing of nanoring composed of one nanoring and two nanotubes. For the constrained case, simulating nanomaile, the left and right regions of the ring were held fixed as shown.

C. Young's modulus, tensile strength and effective mass density

In a standard calculation of the Young's modulus of nanotubes, a tensile load is applied to either end. For nanorings, however, direct application of the load to individual carbon atoms leads to locally extreme tensile stresses and catastrophic failure. To avoid this, two (5, 5) nanotubes were inserted into the nanoring as a tension frame, and a force was applied on the ends of these nanotubes in order to deform the structure. This setting idealizes the loading experienced by one link in a nanochain and is shown in Fig. 5. A second type of simulation considered the effect of left and right constraints on the extension of the nanoring in order to better understand the mechanical response of nanomaile. The position of small regions of carbon atoms at left and right were therefore fixed as shown in the same figure.

MD simulations of nanoring deformation were performed at 100 K in time steps of 0.25 fs. The loading rate was set to 0.002 Å per MD step which corresponds to a strain rate of 2×10^{11} s. To assess the effect of loading rate on the results, a series of intermediate structures in the MD trajectory were selected and annealed in order to obtain potential energies not affected by the rate of strain. Structures were annealed at 100 K for 6.25 ps. A tension rate 4×10^{10} s was chosen for the tensile strength calculation. The ring was loaded, and the time slice just before rupture was selected for annealing at 100 K for 6.25 ps. The resulting structure was then used as an initial condition for the calculation of tensile strength. Tensile strain was calculated using $\varepsilon=(L-L_0)/L_0$ where L_0 is the initial nanotube length (ring circumference) and L is the current nanotube length (ring circumference).

The cross-sectional area of nanotubes is an important parameter in the calculation of Young's modulus. The standard view, accepted in the present work, is that a SWNT may be viewed as a cylindrical shell. Then cross-sectional area is given by $S=\pi dh$ where d and h are the diameter and wall thickness of a SWNT.[32,45–47] The wall thickness, h, is not well defined for a SWNT, but it is reasonable to use the interwall separation of graphite for this parameter.[32] This value, $h=3.354$ Å, is the same as the distance between the layers of MWNTs and leads to estimates of the Young's modulus which are consistent with experimental measurements.[45] One exception to approach is the earlier work of Yakobson, Brabec, and Bernholc, wherein a value of $h=0.66$ Å was derived along with a nonphysical Young's modulus of 5.5 TPa.[48] A second variation in methodology was considered by Cornwell and Wille, who generated molecular dynamics estimates for the Young's moduli based on the assumption of a solid cylindrical cross section.[49] Their approach, though, gives a Young's modulus that varies with tube radius and is therefore viewed as not providing intrinsic strength information about SWNTs.

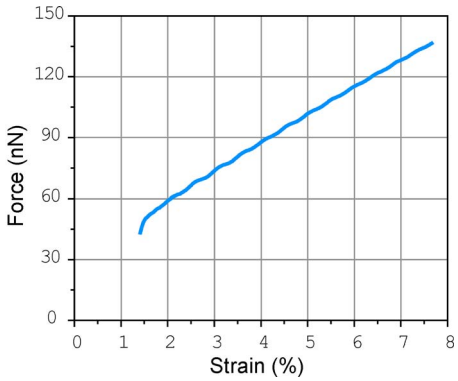

FIG. 6. (Color online) Force vs strain curve for tensile loading of a (10,10) SWNT.

The cross-sectional area of a nanoring is taken to be twice the cross-sectional area of a SWNT. The tensile stress is then $\sigma=F/S$, where F is the applied force. Since the mechanical response is nonlinear for the nanoring, the elastic Young's modulus is defined differentially. The ultimate tensile strength, σ_{UTS}, and Young's modulus, E, are therefore given by

$$\sigma_{\mathrm{UTS}}=\frac{F_{\max}}{nS},\quad E=\frac{\partial\sigma}{\partial\varepsilon}. \tag{1}$$

Here $F_{\max}$ is the ultimate tensile force and $n=1$ and 2, respectively, for the nanotube and nanoring.

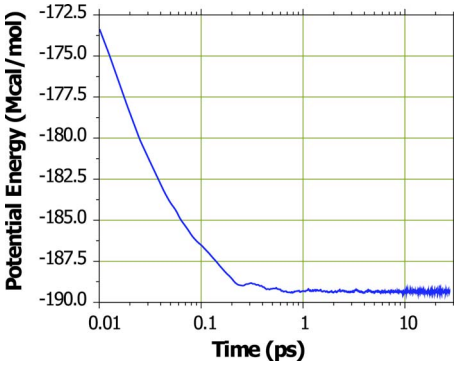

FIG. 7. (Color online) Potential energy of the nanoring as a function of time following initial formation. As indicated by the plot, the energy equilibrates within 1 ps, but the simulation was carried out to 25 ps to ensure that the configuation was stable. The temperature of this simulation is 500 K.

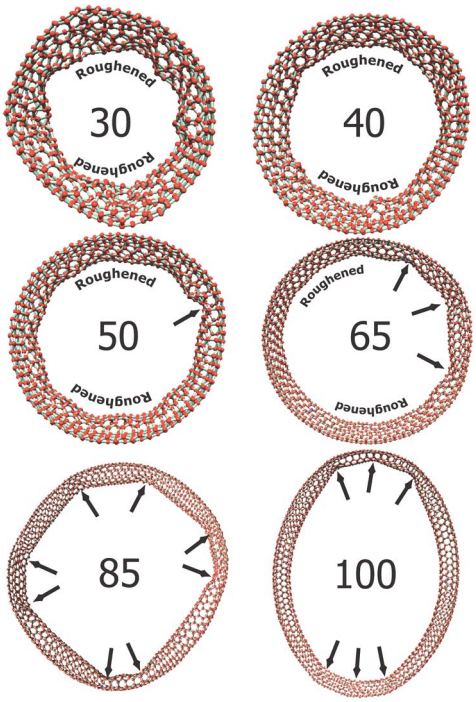

FIG. 8. (Color online) The equilibrated shapes of (5, 5) nanorings with unit repetition lengths of 30, 40, 50, 65, 85, and 100. The rings take on a beltlike geometry with dented inner surfaces. Arrows indicate points identified as dents.

Consistent with the choice of cross-sectional area used in CNT analyses, the mass density of tubes and rings is taken to be

$$\rho = \frac{Nm}{nSl}, \tag{2}$$

where N and m are the number and mass of carbon atoms. l is the length of nanotube and nanoring. The mass density of the nanorings is then 1.467×10^3 Kg/m^3.

III. RESULTS

A. Validation of the MD force field

The force-strain curve of a SWNT is shown in Fig. 6 from which the average Young's modulus was estimated to be 1.047 TPa. This is in good agreement with other theoretical and experimental results, an MD estimate of 1.03–1.04 TPa for a nanotube thickness=0.335 nm;[32] an MD estimate of 0.972 TPa for a nanotube thickness=0.34 nm;[47] a tight binding method approximation of 1.24 TPa for a nanotube thickness of 0.34 nm;[50] and an experimental value of 1.25 TPa obtained for SWNT's with diameters of 1.0–1.5 nm.[51]

B. Equilibrated shape

Figure 7 shows the evolution of potential energy during annealing at 500 K and indicates that the system has reached an equilibrium state after approximately 1 ps. This energy level is maintained for the remainder of the 25 ps simulation.

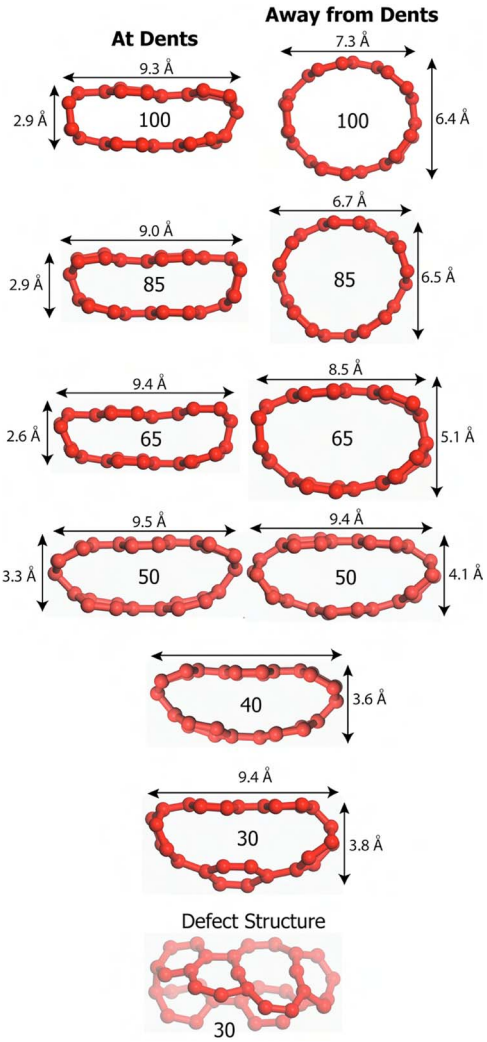

FIG. 9. (Color online) Cross-sectional views of (5, 5) nanorings with unit repetition lengths of 30, 40, 50, 65, 85, and 100. The rings take on a beltlike geometry with dented inner surfaces.

The equilibrated geometry and other (5, 5) rings are shown in Figs. 8 and 9. The ring takes on a beltlike geometry in order to minimize the distortion of carbon-carbon bonds. While the inner side of nanoring is somewhat dented after equilibration, carbon bonding connections do not change from those of the unequilibrated ring and no kinks develop. The same result was obtained in a series of simulations performed between 200 K and 1000 K. The curvature of the nanoring is relatively high due to the short length of the nanotube used, and an even more circular cross section is expected for nanorings with a greater circumference. The lack of kinking is in contrast to that reported elsewhere for which a Brenner-Tersoff potential yielded a kinked nanoring structure for the same initial geometry.[23] Specifically, Hod and Rabani found that (5, 5) nanorings, formed in the same way as in the current study, developed kinks if made of less than 180 unit cells. The complicated nature of both Brenner-Tersoff and ReaxFF potentials makes it difficult clearly identify the source of the discrepancy; however, the Brenner-Tersoff potential sharply breaks the C-C bond when the C-C distance is greater than 1.8 angstroms, while ReaxFF gives a

FIG. 10. (Color online) Tensile loading of nanoring without side constraints.

much smoother description of the C-C bond in that region—in agreement with *ab initio* calculations. Because of this, the Brenner-Tersoff potential introduces a large artificial force when bonds are stretched far beyond their equilibrium values. This may be the cause of the kinks observed. In addition to the distinction between the potentials in the way bonds are described, ReaxFF properly describes transition states relevant to fullerenes while the Brenner-Tersoff potential tends to put them at very high energies. This also tends to imply that ReaxFF model would give more accurate results. A more detailed comparison with quantum mechanical calculations is needed, though, to firmly assess the physicality of nanoring kinks.

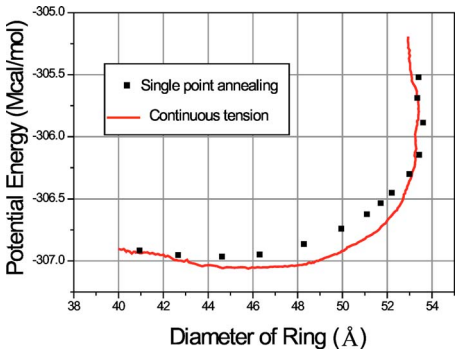

FIG. 11. (Color online) Potential energy vs strain curve for tensile loading of nanoring without side constraints.

It may be, though, that both kinked and unkinked structures are stable for rings with only 50 unit cells. This would be consistent with the work of Gao *et al.*[24] who studied the stability of (10, 10) nanorings. Using an MSFF force field they identified three critical radii associated with the structural stability,

(i) $R < R_b = 38.9$ Å, toroidal structures are not stable;

(ii) $R_b \leqslant R < R_s = 183.3$ Å, both kinked and smooth rings are stable;

(iii) $R_s \leqslant R$, only smooth rings are stable.

Between R_k and R_s, where both kinked and smooth structures are stable, the kinked structures have a lower free energy. It makes sense that a similar regime should exist for the (5, 5) rings as well and that the limits of this regime should be much lower than those associated with the (10, 10) structures. That would be consistent with the conclusion of Hod and Rabani that the value of R_s decreases with tube diameter. We therefore posit that (5, 5) nanorings with 50 unit cells (39.2 Å) are in the range between the (5, 5) values of R_k and R_s.

The (5, 5) rings shown in Figs. 8 and 9 also indicate a trend in cross-sectional shape. Rings below 25 repetition units were found to be unstable, and even the (5, 5, 30) ring was found to have broken bonds, as shown in Fig. 9. The (5, 5, 40) ring has a stable shape but with a roughened interior. As the number of repeat units increases, though, rings tend to

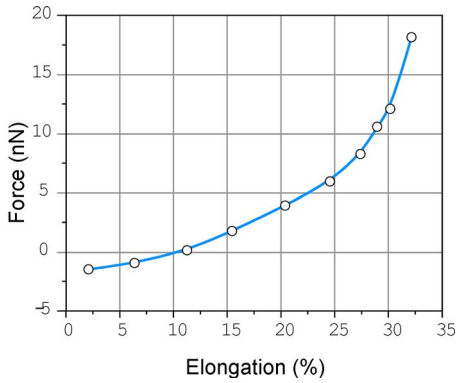

FIG. 12. (Color online) Force vs strain curve for tensile loading of a nanoring without side constraints.

FIG. 13. (Color online) Tensile loading of nanoring with side constraints.

take on a bimodal shape with dented regions that have a more deformed cross-sectional area. Away from such dents, the rings tend to be more circular in cross section. This bimodal character tends to become more extreme as the number of repeat units increases.

C. Young's modulus

Figure 10 shows the deformation process of a nanoring without side constraints. The nanoring surface becomes smoother with bond elongation but bonding connections do not change. Figure 11 shows the associated plot of potential energy versus strain. At the beginning and end of the loading curve, the equilibrated potential energy of a single point of the MD trajectory is quite close to that obtained under dynamic loading.

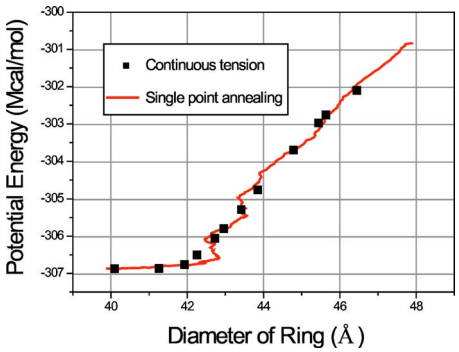

FIG. 14. (Color online) Potential energy vs strain curve for tensile loading of nanoring with side constraints.

Figure 12 shows the force-strain curve for nanoring deformation. The unconstrained nanoring ruptures at a force of 18 nN. By way of comparison, nanohooks fail at approximately 3 nN.[14] For strains less than 20%, the relationship between force and strain is approximately linear, and from this curve the Young's modulus of the unconstrained nanoring was estimated to 19.43 GPa—about 2% of the value for a single nanotube. For strains larger than 25%, the Young's modulus is 121.94 GPa—about 12% of the value for a single nanotube.

Figure 13 shows the deformation process for a constrained nanoring. The deformation behavior is similar to the case with no constraint, and here again the structure is stable throughout the deformation. Significant structural distortion was observed around the fixed atoms though. Figure 14 shows the potential energy versus strain curve under the constrained condition. Unlike the case without any constraints, the equilibrated potential energy of the constrained case is quite closed to the continuous loading curve. The deformation is primarily distributed in bond-length change which corresponds to the end part of the unconstrained case. Figure 15 shows the force-strain curve of nanoring deformation under constrained conditions. Similar to the case with no such constraint, under small strain (less than 3%) the relationship between force and strain is approximately linear and the Young's modulus of constrained nanoring is 124.9 GPa. This value is about six times of the value of unconstrained one

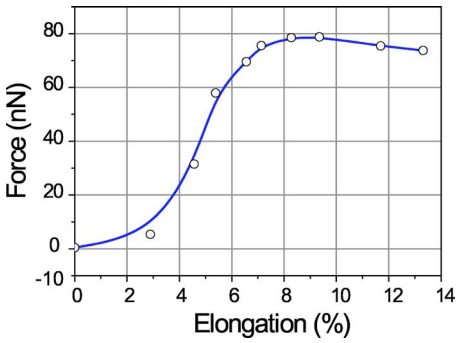

FIG. 15. (Color online) Force vs strain curve for tensile loading of nanoring with side constraints.

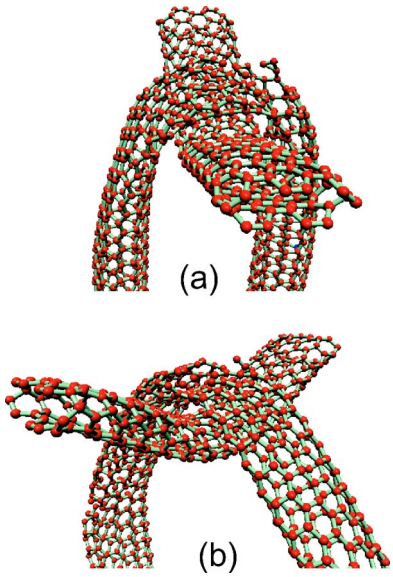

FIG. 16. (Color online) The structure of nanorings at failure, (a) without constraints (nanochain), (b) with constraints (nanomaile).

(19.43 GPa), however it is still much lower than that of the single nanotube—approximately 1 TPa. At strains higher than 3%, the Young's modulus is approximately 1.55 TPa—nearly 50% higher than that of the SWNT.[4]

D. Tensile strength

In order to remove the effect of loading rate on the tensile strength calculation, a very low rate was applied at the end of the initial deformation. Figure 16 shows the breaking structure of both the constrained and unconstrained nanoring. It can be seen that cracks originate from the outside of the nanoring under both types of loading. The outer carbon-carbon bonding length is larger than that inside, and the outer bonding is less stable than that inside during the deformation. For both types of loading, ring failure initiates within the interaction area between nanotubes and the nanoring.

Figure 17 shows the force-strain curve with slow tensile loading for both structures. When some carbon-carbon bonds are finally broken, the tensile force drops dramatically. However, the *crack* does not extend very quickly and further deformation required with additional tensile loading. This implies that the nanoring structure has a high resistance to crack extension. From the figure, it is estimated that the tensile strengths of the unconstrained and constrained nanorings are 5.72 GPa and 8.52 GPa, respectively. These numbers are compared with those of several other common materials in Table I.

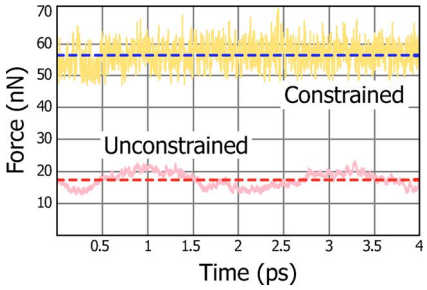

FIG. 17. (Color online) Force vs time curves for loaded nanorings (constrained and unconstrained) under tensile loads just below that determined to cause failure.

TABLE I. Tensile strength of typical materials.

Material	Tensile strength (GPa)
Nanoring	5.7
Nanomaile	8.5
Steel	0.8–1.4 (Ref. 53)
Aluminum	0.14 (Ref. 53)
Spider silk	1.3 (Ref. 52)
CNT composite	0.16 (Ref. 57)
CNT fibers	9–15 (Ref. 9)
Single CNT	150 (Ref. 54)

E. Strength-to-density ratio

The mass density of nanorings is extremely low. The tensile strength to density ratio is the 3.89×10^6 N−m/K g (nanochain) and 5.81×10^6 N−m/K g (nanomaile), and these values are compared with those for other materials in Table II.

F. Flexibility

Perhaps the most important property of nanoring structures is their flexibility. Table III lists the maximum strain of a number of classical materials for comparison, where it is seen that the nanoring values are on the same order as polycrystalline aluminum and steel. Unlike these metallic systems, however, the nanoring deformation is completely reversible; nanochains and nanomaile will recover their original shape when the external loading is removed. For example, Fig. 18 shows the complete and stable recovery of a highly deformed nanoring. Nanochains and nanomaile therefore offer the possibility of creating macroscopic struc-

TABLE II. Tensile strength to mass density ratio of typical materials.

Material	Strength/Density (MJ/kg)
Nanoring	3.9
Nanomaile	5.8
Steel	0.11–0.18 (Ref. 53)
Aluminum	0.05 (Ref. 53)
Spider silk	0.9 (Ref. 52)
CNT composite	0.015 (Ref. 57)
CNT fiber	6–10 (Ref. 9)
Single CNT	60 (Refs. 54,55)

TABLE III. Maximum strain of selected materials.

Material	Max strain (%)	Reversible
Nanochain	39	Yes
Nanomaile	25.2	Yes
Steel	25 (Ref. 53	No
Aluminum	4053	No
Spider silk	47653	Yes
Single CNT	3054 and 55	Yes

tures with the unique, dual character of high strength and superior flexibility.

The large strains of the metallics is due, of course, to the motion of dislocations implying that the strain rates must be relatively low in order to achieve the maximum strains listed. No such strain rate limitations would exist for the nanoring structures.

IV. DISCUSSION

A reactive force field, molecular dynamics model (ReaxFF) was used to create and mechanically load carbon nanorings. Tensile loading was carried out both with and without side constraints as a means of quantifying the mechanical character of *nanochains* and *nanomaile*, respectively. The influence of defects on the mechanical properties, while certainly important, was not considered here.[56]

The nanoring Young's modulus increases monotonically with strain from 19.43 GPa to 121.94 GPa (nanochains) and from 124.98 GPa to 1559.9 GPa (nanomaile). An unconstrained (5, 5) nanoring with 1000 carbon atoms was found to rupture at a force of 18 nN as compared with a 3 nN limit of nanohooks.[14] The tensile strength to mass density was estimated to be 1.46–3.89 MJ/kg. This value is approximately 15–20 times that of steel and 1.5–4 times that of spider silk. The maximum strain is about 39% (nanochains) and 25.2% (nanomaile), and these deformations are completely reversible.

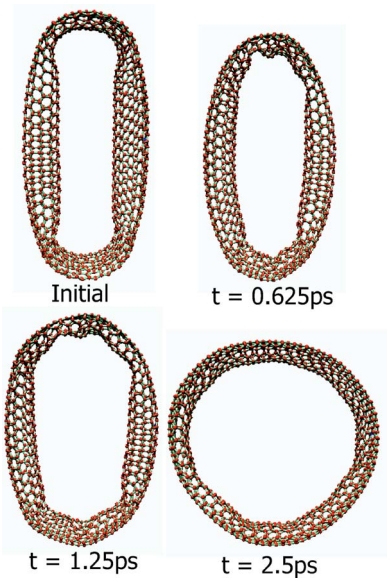

FIG. 18. (Color online) The load on a highly deformed nanoring is released, and it quickly recovers its original, toroidal shape.

*Electronic address: mlusk@mines.edu

[1] H. Ye, H. Lam, N. Titchenal, Y. Gogotsi, and F. Ko, Appl. Phys. Lett. **85**, 1775 (2004).
[2] R. G. Saito Dresselhaus, and M. S. Dresselhaus, *Physical Properties of Carbon Nanotubes* (Imperial College, London, 1998).
[3] P. J. P. Harris, *Carbon Nanotubes and Related Structures: New Materials for the Twenty-First Century* (Cambridge University Press, Cambridge, UK, 1999).
[4] M. M. J. Treacy, T. W. Ebbesen, and J. M. Gibson, Nature (London) **381**, 678 (1996).
[5] L. S. Schadler, S. C. Giannaris, and P. M. Ajayan, Appl. Phys. Lett. **73**, 3842 (1998).
[6] X. Xu and M. M. Thwe, Appl. Phys. Lett. **81**, 2833 (2002).
[7] Y. Ren, Y. Q. Fu, and K. Liao, Appl. Phys. Lett. **84**, 2811 (2004).
[8] A. G. Rinzler, J. Liu, H. Dai, P. Nikolaev, C. B. Huffman, F. J. Rodriguez-Macias, P. J. Boul, A. H. Lu, D. Heymann, D. T. Colbert, R. S. Lee, J. E. Fischer, A. M. Rao, P. C. Eklund, and R. E. Smalley, Appl. Phys. A: Mater. Sci. Process. **A67**, 29 (1998).
[9] B. Vigolo, A. Penicaud, and C. Coulon, Science **290**, 1331 (2000).
[10] M. L. Lake and G. G. Tibbetts, AIP Conf. Proc. **723**, 455 (2004).
[11] A. B. Dalton, S. Collins, E. Muñoz, J. M. Razal, V. H. Ebron, J. P. Ferraris, J. N. Coleman, B. G. Kim, and R. H. Baughman, Nature (London) **423**, 703 (2003).
[12] H. W. Kroto, J. R. Heath, S. C. O'Brien, R. F. Curl, and R. E. Smalley, Nature (London) **318**, 162 (1985).
[13] K. Miura, S. Kamiya, and N. Sasaki, Phys. Rev. Lett. **90**, 055509 (2003).
[14] S. Berber, Y. K. Kwon, and D. Toma'nek, Phys. Rev. Lett. **91**, 165503 (2003).
[15] S. Iijimaa, M. Yudasakaa, R. Yamadaa, S. Bandowb, K. Suenagab, F. Kokaic, and K. Takahashic, Chem. Phys. Lett. **309**, 165 (1999).
[16] Z. Yao, H. W. C. Postma, L. Balents, and C. Dekker, Nature (London) **402**, 273 (1999).
[17] B. I. Dunlap, Phys. Rev. B **46**, R1933 (1992).
[18] S. Itoh, S. Ihara, and J. I. Kitakami, Phys. Rev. B **47**, R1703 (1993).
[19] V. Meunier, Ph. Lambin, and A. A. Lucas, Phys. Rev. B **57**, 14886 (1998).
[20] E. C. Kurby, R. B. Mallion, and P. Pollak, J. Chem. Soc. Dalton Trans. **89**, 1945 (1993).
[21] G. Gao, T. Cagin, and William A. Goddard III, *Seventh foresight conference on molecular nanotechnology*, Santa Clara, CA, 1999.
[22] L. Liu, C. S. Jayanthi, and S. Y. Wu, Phys. Rev. B **64**, 033412 (2001).
[23] O. Hod, E. Rabani, and R. Baer, Phys. Rev. B **67**, 195408 (2003).

[24] Y. J. Guo, N. Karasawa, and W. A. Goddard III, Nature (London) **351**, 464 (1991).
[25] J. Liu, H. Dai, J. H. Hafner, D. T. Colbert, and R. E. Smalley, Nature (London) **385**, 780 (1997).
[26] M. Sano, A. Kamino, J. Okamura, and S. Shinkai, Science **293**, 1299 (2001).
[27] R. Martel, H. R. Shen, and P. H. Avouris, J. Phys. Chem. B **103**, 7551 (1999).
[28] P. H. Avouris, T. Hertel, R. Martel, T. Schmidtn, H. R. Shea, and R. E. Walkup, Appl. Surf. Sci. **141**, 201 (1999).
[29] L. Liu, G. Y. Guo, C. S. Jayanthi, and S. Y. Wu, Phys. Rev. Lett. **88**, 217206 (2002).
[30] N. Yao, and V. Lordi, J. Appl. Phys. **84**, 1939 (1998).
[31] B. Ni, S. B. Sinnott, P. T. Mikulski, and J. A. Harrison, Phys. Rev. Lett. **88**, 205505 (2002).
[32] K. M. Liew, X. Q. He, and C. H. Wong, Acta Mater. **52**, 2521 (2004).
[33] J. W. Che, T. Cagin, and W. A. Goddard III, Nanotechnology **10**, 263 (1999).
[34] B. I. Yakobson, M. P. Campbell, C. J. Brabec, and J. Bernhole, Comput. Mater. Sci. **8**, 341 (1997).
[35] B. I. Yakobson, C. J. Brabec, and J. Bernholc, Phys. Rev. Lett. **76**, 2511 (1996).
[36] Z. Mao and S. B. Sinnott, J. Phys. Chem. B **105**, 6916 (2001).
[37] B. Ni and S. B. Sinnott, Phys. Rev. B **61**, R16343 (2000).
[38] D. W. Brenner, Phys. Rev. B **42**, 9458 (1990).
[39] R. C. Mowrey, D. W. Brenner, B. L. Dunlap, J. W. Mintmire, and C. T. White, J. Phys. Chem. **95**, 7138 (1991).
[40] D. W. Brenner, J. A. Harrison, C. T. White, R. J. Colton, and J. A. Harrison, Thin Solid Films **206**, 220 (1991).
[41] D. W. Brenner *et al.*, J. Phys.: Condens. Matter **14**, 783 (2002).
[42] A. C. T. van Duin, S. Dasgupta, F. Lorant, and W. A. Goddard III, J. Phys. Chem. A **105**, 9396 (2001).
[43] J. J. P. Stewart, J. Comput. Chem. **10**, 221 (1989).
[44] K. D. Nielson, A. C. T. van Duin, J. Oxgaard, W. Q. Deng, and W. A. Goddard III, J. Phys. Chem. A **109**, 493 (2005).
[45] Xin Zhou, Jianjung Zhou, and Ou-Yang Zhong, Phys. Rev. B **62**, 13692 (2000).
[46] V. N. Popov, V. E. VanDoren, and M. Balkanski, Phys. Rev. B **61**, 3078 (2000).
[47] J. P. Lu, Phys. Rev. Lett. **79**, 1297 (1997).
[48] B. I. Yakobson, C. J. Brabec, and J. Bernholc, Phys. Rev. Lett. **76**, 2511 (1996).
[49] C. F. Cornwell, and L. T. Wille, Solid State Commun. **101**, 555 (1997).
[50] E. Hernández, C. Goze, P. Bernier, and A. Rubio, Phys. Rev. Lett. **80**, 4502 (1998).
[51] A. Krishnan, E. Dujardin, T. W. Ebbesen, P. N. Yianilos, and M. M. J. Treacy, Phys. Rev. B **58**, 14013 (1998).
[52] Z. Shao and F. Vollrath, Nature (London) **418**, 741 (2002).
[53] *SM Engineered Materials Reference Book*, 2nd ed., edited by M. Bauccio (ASM International, Materials Park, OH, 1994).
[54] M. F. Yu, L. Oleg, M. J. Dyer, K. Moloni, T. F. Kelly, and R. S. Ruoff, Science **287**, 637 (2000).
[55] B. G. Demczyk, Y. M. Wang, J. Cumings, M. Hetman, W. Han, A. Zettl, and R. O. Ritchie, Mater. Sci. Eng., A **334**, 173 (2002).
[56] L. Chico, V. H. Crespi, L. X. Benedict, S. G. Louie, and M. L. Cohen, Phys. Rev. Lett. **76**, 971 (1996).
[57] D. Qian, E. C. Dickey, R. Andrews, and T. Rantell, Appl. Phys. Lett. **76**, 2868 (2000).